Conference paper

Vincenzina Barbera, Andrea Bernardi, Alberto Palazzolo, Alessandro Rosengart, Luigi Brambilla and Maurizio Galimberti*

Facile and sustainable functionalization of graphene layers with pyrrole compounds

https://doi.org/10.1515/pac-2017-0708

Abstract: A facile and sustainable functionalization of graphene layers was performed with pyrrole compounds (PyC) prepared through the Paal–Knorr reaction of a primary amine with 2,5-hexanedione. A good number of primary amines were used: hexanamine, dodecanamine, octadecanamine, 2-aminoacetic acid, 2-amino-1,3-propanediol, 3-(triethoxysilyl)propan-1-amine. The reactions were characterized by good yield, up to 96 %, and indeed satisfactory atom efficiency, up to 80 %. The functionalization of graphene layers was obtained by mixing PyC with a high surface area graphite and heating at a temperature range from 130 °C to 150 °C for 3 h. The yield of functionalization reaction was larger than 60 % and also up to about 90 % for the pyrrole compounds from dodecanamine and 2-amino-1,3-propanediol, respectively. The cycloaddition reaction between the graphene layers and the pyrrole compound, oxidized in two position, is proposed as working hypothesis to account for such efficient functionalization. Raman spectroscopy revealed that the structure of the graphitic substrate remained substantially unaltered, after the reaction. Stable dispersions of HSAG adducts with different PyC were prepared in solvents with different solubility parameters and HRTEM analysis showed the presence of aggregates of only few layers of graphene. Qualitative results of dispersion tests were used to calculate the Hansen sphere for the HSAG adduct with the pyrrole compound based on dodecanamine so to provide a first estimate of its Hansen solubility parameters. This work paves the way for the facile and sustainable modification of the solubility parameters of graphene layers and for the predictive assessment of their compatibility with different environments.

Keywords: functionalization; graphene layers; ICGC-6; Paal–Knorr reaction; pyrrole compounds; solubility parameters.

Introduction

Graphene (G) [1–4] is the one carbon atom thick graphitic material and has indeed exceptional properties: high charge-carrier mobilities [5, 6], in-plane thermal conductivity [7], very high elastic modulus, theoretically over 1 TPa, and Young modulus, about 1060 MPa [8]. The polymeric nature of graphene layer with the six atoms aromatic ring as the repeating unit is responsible for such exceptional properties. Hence, main objectives of graphene synthesis [8–12] and functionalization [8, 13–23] are to obtain and preserve such structure.

Impressive research activity is performed for the preparation of nanocomposites based on graphene and graphene-related materials (GRM) [24, 25], as composites can bring to the macroscopic scale the properties of

Article note: A collection of invited papers based on presentations at the 6th International IUPAC Conference on Green Chemistry (ICGC-6), Venice (Italy), 4–8 September 2016.

***Corresponding author: Maurizio Galimberti,** Politecnico di Milano, Department of Chemistry, Materials and Chemical Engineering "G. Natta", Via Mancinelli 7, 20131 Milano, Italy, e-mail: maurizio.galimberti@polimi.it
Vincenzina Barbera, Andrea Bernardi, Alberto Palazzolo, Alessandro Rosengart and Luigi Brambilla: Politecnico di Milano, Department of Chemistry, Materials and Chemical Engineering "G. Natta", Via Mancinelli 7, 20131 Milano, Italy

graphene. Applications of nanocomposites are studied in particular for energy storage devices [26], catalyst supports and fuel cells [27], sensors and actuators [28], chemical filters and membranes [29], structural composites [30], biosensors [31] and artificial bone tissues [32]. G and GRM are also increasingly used in the field of catalysis [33, 34]. It is well known that carbocatalysis promotes synthesis and transformation of organic or inorganic substrates [35].

It is widely acknowledged that ultimate dispersion of graphene layers in the composite is mandatory to fully exploit G and GRM properties. Such an objective can be achieved by using mechanical energy, but at the expenses of G structure, or relying on the compatibility of G with the surrounding matrix. The latter approach requires the functionalization of the graphene layers.

The first objective of the present work was to functionalize graphene layers with a simple, sustainable, environmentally friendly and economically viable method, suitable for large scale development, preserving the ideal graphene structure. As a further challenging objective, such method had to be versatile, suitable to introduce families of functional groups onto the graphene layers, and had to allow the tuning of their solubility parameter. These objectives were pursued by using heterocyclic molecules.

Heterocyclic chemistry is an important field in synthetic organic chemistry. Nitrogen containing compounds are very widespread in nature and, among them, particularly relevant are pyrrole based molecules. These are involved in the synthesis of natural products and play an important pharmacological role. On this background, the synthesis of pyrrole derivatives is indeed a hot topic.

Classical methods for the synthesis of pyrroles are Piloty [36] Paal–Knorr [37, 38], Barton–Zard [39], and Hantzsch [40], syntheses. Nowadays, new approaches involving the use of transition-metal intermediates [41], multicomponent reactions [42], and reductive couplings [43] are documented. The most used procedure is still the Paal–Knorr reaction [37, 38]. Paal and Knorr independently used 1,4-dicarbonyl compounds, primary amine and weak mineral acid catalyst. Since then, many variations of the synthetic procedure have been developed, mainly by using various acidic reagents (e.g. HCl [44], p-toluenesulfonic acid [45]). The advent of green chemistry led to develop environmentally friendly procedures, with the use of surfactants in water [46], inorganic compounds (e.g. clay) [47], ionic liquids [48], mechanical activation, [49] ultrasounds [50].

In our research group, sustainable synthesis of a pyrrole derivative was obtained [51, 52], based on the reaction of primary amine with diketone in the absence of any solvent and catalyst. 2-(2,5-Dimethyl-1*H*-pyrrol-1-yl)-1,3-propanediol (serinol pyrrole, SP) was obtained from the reaction of 2-amino-1,3-propandiol (known as serinol) with 2,5-hexanedione (HD). Serinol pyrrole has been then used as the heterocyclic molecule for the functionalization of sp^2 carbon allotropes [20] and of graphene layers among them. Very high functionalization yield was reported and stable water dispersions of the carbon materials were obtained [21, 22]. The high efficiency of the functionalization reaction paved the way to explore the reaction of the carbon allotropes with pyrrole compounds other than serinol pyrrole. In this paper, the synthesis of pyrrole compounds obtained from 2,5-HD and primary amines other than serinol is reported. The following primary amines were used: hexanamine, dodecanamine, octadecanamine, 2-aminoacetic acid, 3-(triethoxysilyl)propan-1-amine. Amine-derived pyrrole compounds (PyC) were then used for the functionalization reaction of high surface area graphite (HSAG) endowed with a surface area of 300 m^2/g, a low number of layers stacked in crystalline domain (about 35), a high order inside the plane and thus a high shape anisotropy [53]. The functionalization reaction is described and the main characteristics of the adducts of HSAG with the pyrrole compounds are discussed. Characterizations were performed by means of Fourier transformed infrared (FT-IR) and Raman spectroscopies. Dispersions of functionalized HSAG were prepared in solvents with different solubility parameters, from water to ethyl acetate to n-heptane, and their stability was inspected over weeks as storage time. The objective was to investigate the ability of PyC to modify the solubility parameter of the graphene layers. The concept of solubility parameter has been already applied to nano-carbon materials, such as nanotubes [54], carbon fibers [55], and graphene [56]. It has been shown [54] that a solvent able to minimize the Gibbs free energy of mixing with graphene and carbon nanotubes is able to promote the debundling of the tubes and the exfoliation of graphene aggregates. Moreover, matching the solubility parameters of polymer matrix and CNT leads to easier percolation of the nanofiller and

to larger electrical conductivity [57]. In the present work, the qualitative results of the dispersion tests were used to calculate the Hansen sphere for the HSAG adduct with the PyC based on dodecylamine, performing a first estimate of the Hansen solubility parameters (HSP) [58] of the adduct. High resolution transmission electron microscopy was performed on graphene layers taken from the dispersions and aggregates made by few layers of graphene were identified.

Experimental

Materials

Reagents and solvents for the preparation of pyrrole based compounds

All reagents and solvents were commercially available and were used without further purification. 2,5-Hexanedione, 2-amino-1,3-propanediol, hexanamine, dodecanamine, octadecanamine, 3-(triethoxysilyl)propan-1-amine, 2-aminoacetic acid, acetone, ethyl acetate, toluene, 2-propanol, heptane, methanol, 2-butanol, tetrahydrofuran, p-xylene, deuterated chloroform ($CDCl_3$) and dimethylsulfoxide (DMSO-*d*6) were from Sigma-Aldrich.

High surface area graphite

Synthetic Graphite 8427® from Asbury Graphite Mills Inc. was used. The technical data sheet reports carbon content of at least 99 wt% and surface area equal to 330 m^2/g. Chemical composition, determined from elemental analysis, on HSAG sample washed with acetone, was (as mass %): carbon 99.5, hydrogen 0.4, nitrogen 0.1, oxygen <0.5. Further characterization has been reported elsewhere. The lateral size of graphitic layers was observed in TEM micrographs to be in the range from about 300 nm to more than 1 micron [23]. The number of layers stacked in crystalline domain was calculated, from XRPD, to be about 35 [23, 53]. This means that the thickness of crystallites in pristine HSAG was of about 12 nm.

Synthesis of pyrrole derivatives

Metrics of the synthesis

The atom economy (AE) is given by the ratio of the molar mass of products over the molar mass of reagents. The reaction mass efficiency (RME) is the product of yield, atom economy and the inverse of the stoichiometry factor [59].

Synthesis of 1-hexyl-2,5-dimethyl-1H-pyrrole (1)

One gram of hexanamine (9.88 mmol) and 1.1 g of 2,5-hexanedione (9.88 mmol) were poured in a 10 mL glass vial equipped with magnetic stirrer. The mixture was left to stir at 130 °C for 3 h. After this time, the reaction mixture was cooled to room temperature and the water was removed at reduced pressure. Pure product was obtained yielding 1.25 g (73 %). ^{1}H NMR ($CDCl_3$, 400 MHz); δ (ppm) = 5.84 (s, 2H, C$\underline{H}$), 5.75 (s, 2H, C$\underline{H}$), 3.57 (s, 2H, N–C$\underline{H}_2$-C), 3.52 (m, 1H, N–C$\underline{H}$-$(CH_2)_2$), 2.28 (s, 6H, C$\underline{H}_3$), 2.24 (s, 6H, C$\underline{H}_3$), 1.71 (m, 4H, C$\underline{H}_2$), 1.32 (m, 2H, C$\underline{H}_2$), 1.18 (m, 3H, C$\underline{H}_3$), 1.02 (m, 6H, C$\underline{H}_3$). ^{13}C NMR ($CDCl_3$, 100 MHz); δ (ppm) = 128.98, 128.03, 106.37, 106.00, 56.60, 49.56, 48.26, 44.712, 41.82, 39.91, 35.26, 32.68, 27.62, 23.68, 14.22.

Synthesis of 1-dodecyl-2,5-dimethyl-1H-pyrrole (2)

One gram of dodecanamine (5.39 mmol) and 0.62 g of 2,5-hexanedione (5.39 mmol) were placed in 10 mL glass vial equipped with a cap. The reaction mixture was heated to 130 °C and maintained at this temperature under vigorous stirring for 3 h. A dark amber viscous oil was obtained, yielding to 0.99 g (62 %).

^{1}H NMR ($CDCl_3$, 400 MHz); δ (ppm) = 5.75 (s, 2H, C$\underline{H}$), 3.68–3.72 (m, 2H, C$\underline{H}_2$), 2.21 (s, 6H, C$\underline{H}_3$), 1.60 (m, 2H, C$\underline{H}_2$), 1.30 (m, 2H, CH_2–C$\underline{H}_2$–CH_3), 1.26 (m, 18H, CH_2), 0.90–0.86 (t, 3H, CH_3). ^{13}C NMR ($CDCl_3$, 100 MHz); δ (ppm) = 127.2, 104.9, 43.6, 31.9, 31.0, 29.6, 26.9, 22.6, 14.0, 12.4.

Synthesis of 2,5-dimethyl-1-octadecyl-1H-pyrrole (3)

0.5 g of octadecanamine (1.85 mmol) and 0.2 g of 2,5-hexanedione (1.85 mmol) were poured in a 10 mL glass vial equipped with magnetic stirrer. The mixture was left to stir at 130 °C for 3 h. After this time, the reaction mixture was cooled to room temperature. Pure product was obtained yielding 0.518 g (73 %). ^{1}H NMR ($CDCl_3$, 400 MHz); δ (ppm) = 5.81 (s, 2H, C$\underline{H}$), 3.78–3.74 (t, 2H, N–C$\underline{H}_2$–C$\underline{H}_2$–), 2.27 (s, 6H, C$\underline{H}_3$), 1.66 (m, 2H, CH_2–C$\underline{H}_2$–CH_2–R), 1.37 (m, 2H, C$\underline{H}_2$–CH_3) 1.33 (m, 12H, C$\underline{H}_2$), 0.95 (m, 3H, C$\underline{H}_3$). ^{13}C NMR ($CDCl_3$, 100 MHz); δ (ppm) = 127.27, 105.03, 43.72, 32.01, 31.10, 29.78, 27.05, 22.76, 14.16, 12.51.

Synthesis of 2-(2,5-dimethyl-1H-pyrrol-1-yl)acetic acid (4)

One gram of 2-aminoacetic acid (1.85 mmol) and 1.52 g of 2,5-hexanedione (1.85 mmol) were poured in a 100 mL glass round bottom flask equipped with magnetic stirrer. The mixture was left to stir at 130 °C for 3 h. After this time, the reaction mixture was cooled to room temperature. Pure product was obtained yielding 0.605 g (80 %). ^{1}H NMR ($CDCl_3$, 400 MHz); δ (ppm) = 9.68 (1H, COO$\underline{H}$), 5,76 (s, 2H, C$\underline{H}$), 4.47 (s, 2H, C$\underline{H}_2$), 2.14 (s, 6H, C$\underline{H}_3$). ^{13}C NMR ($CDCl_3$, 100 MHz); δ (ppm) = 173.16, 128.02, 105.50, 45.20, 12.28.

Synthesis of 2-(2,5-dimethyl-1H-pyrrol-1-yl)propane-1,3-diol (5)

A mixture of 2,5-hexanedione (41.4 g; 0.36 mol) and serinol (30.0 g; 0.36 mol) was poured into a 100 mL round bottomed flask equipped with magnetic stirrer. The mixture was then stirred, at 150 °C for 3 h. After this time, the reaction mixture was cooled to room temperature. Pure product was obtained yielding 55 g (96 %). ^{1}H NMR ($CDCl_3$, 400 MHz); δ (ppm) = 2.27 (s, 6H); 3.99 (m, 4H); 4.42 (quintet, 1H); 5.79 (s, 2H). ^{13}C NMR (DMSO-*d*6, 100 MHz); δ (ppm) = 127.7; 105.9; 71.6; 61.2; 13.9.

Synthesis of 1-(3-(triethoxysilyl)propyl)-2,5-dimethyl-1H-pyrrole (6)

One gram of 3-(triethoxysilyl)propan-1-amine (4.82 mmol) and 0.55 g of 2,5-hexanedione (4.82 mmol) were poured in a 10 mL glass vial equipped with magnetic stirrer. The mixture was left to stir at 130 °C for 3 h. After this time, the reaction mixture was cooled to room temperature and the water was removed at reduced pressure. Pure product was obtained yielding 1.15 g (80 %).

^{1}H NMR ($CDCl_3$, 400 MHz); δ (ppm) = 5.73 (s, 2H, C$\underline{H}$), 3.80 (m, 6H, O–C$\underline{H}_2$), 3.70 (m, 2H, N–C$\underline{H}_2$), 2.20 (s, 6H, C$\underline{H}_3$), 1.71 (m, 2H, CH_2), 1.22 (m, 2H, C$\underline{H}_2$), 0.62 (m, 3H, C$\underline{H}_3$). ^{13}C NMR ($CDCl_3$, 100 MHz); δ (ppm) = 127.6, 105.6, 56.1, 51.05, 27.01, 19.2, 13.01, 12.51.

Preparation of HSAG-PyC adducts

Synthesis of HSAG-PyC adducts

General procedure

In a 50 mL round bottom flask were put in sequence HSAG (200 mg, 2.8 mmol) and acetone (15 mL). The suspension was sonicated for 15 min, using a 2 L ultrasonic bath. In 5 mL of acetone, 0.28 mmol of PyC one (5 mL)

was added. The resulting suspension was sonicated for 15 min. The solvent was removed under reduced pressure. The black powder of HSAG/PyC was poured into a 25 mL round bottomed flask equipped with magnetic stirrer and was heated at 180 °C for 2 h. After this time, the mixture was placed in a Büchner funnel with a sintered glass disc, thoroughly washed with acetone and then recovered and weighed.

Preparation of adducts with PyC of Table 1

The same procedure was adopted for the preparations of all the adducts presented in this manuscript. In all preparations, 200 mg of HSAG were used. Adducts were obtained as a black powder. Functionalization yield was determined through the following equation (eq. 1):

$$\text{Functionalization yield (\%)} = 100 * \frac{\text{PyC mass \% in (HSAG-PyC adduct) after acetone washing}}{\text{PyC mass \% in (HSAG-PyC adduct) before acetone washing}} \quad (1)$$

%mass of PyC in HSAG-PyC adduct (before and after acetone washing) were obtained from TGA analysis, as the mass loss in the temperature range from 150 °C to 700 °C. Data are shown in Table 2 below in the text.

Preparation of HSAG-SP. Forty-seven microgram of SP were used. Theoretical mass % of SP in the adduct: 19. Functionalization yield: 87.2 %. Functionalization yield was calculated on the basis of TGA results, according to eq. (1), by applying the following procedure.

- SP mass % in HSAG-SP adduct before acetone washing = 15.4 – 0.5 = 14.9
- SP mass % in HSAG-SP adduct after acetone washing = 13.5 – 0.5 = 13
- 0.5 % is the mass loss of HSAG after acetone washing.

Functionalization yield = 100 × (SP mass % in HSAG-SP adduct after acetone washing)/(SP mass % in HSAG-SP adduct before acetone washing) = 100 × (13/14.9) = 87.2 %.

Preparation of HSAG-DDcP. Seventy-three microgram of DDcP were used. Theoretical mass % of DDcP in the adduct: 26.7. Functionalization yield: 73.0 %.

Preparation of HSAG-Gly. Forty-two microgram of Gly were used. Theoretical mass % of Gly in the adduct: 17.3. Functionalization yield: 61.3 %.

Preparation of HSAG-APTESP. Eighty-four microgram of APTESP were used. Theoretical mass % of APTEPS in the adduct: 29.5. Functionalization yield: 69.7 %.

Characterization of HSAG adducts

Thermogravimetric analysis

TGA tests under flowing N_2 (60 mL/min) were performed with a Mettler TGA SDTA/851 instrument according to the standard method ISO9924-1. Samples (10 mg) were heated from 30 to 300 °C at 10 °C/min, kept at 300 °C for 10 min, and then heated up to 550 °C at 20 °C/min. After being maintained at 550 °C for 15 min, they were further heated up to 700 °C and kept at 700 °C for 30 min under flowing air (60 mL/min).

Fourier transform-infra red spectroscopy (FT-IR)

The IR spectra were recorded in transmission mode (128 scan and 4 cm^{-1} resolution) placing a small amount of powder sample in a Diamond Anvil Cell (DAC) using a ThermoElectron Continuμm IR microscope coupled with a FT-IR Nicolet Nexus spectrometer.

Raman spectroscopy

Raman spectra of powder samples deposited on a glass slide were recorded with a Horiba Jobin Yvon Labram HR800 dispersive Raman spectrometer equipped with Olympus BX41 microscope and a 50X objective. The excitation line at 632.8 nm of a He/Ne laser used for the experiments was kept at 0.5 mW in order to prevent samples degradation. Spectra were recorded as the average of four acquisitions (scan time: 30 s each) with a spectral resolution of 2 cm^{-1}.

High-resolution transmission electron microscopy (HRTEM)

HRTEM investigations on HSAG samples were carried out with a Philips CM 200 field emission gun microscope operating at an accelerating voltage of 200 kV. Few drops of the suspensions were deposited on 200 mesh lacey carbon-coated copper grid and air-dried for several hours before analysis. During acquisition of HRTEM images, the samples did not undergo structural transformation. Low beam current densities and short acquisition times were adopted. To estimate the number of stacked graphene layers and the dimensions of the stacks visible in HRTEM micrographs, the Gatan Digital Micrograph software was used.

Preparation and characterization of dispersions of HSAG-PyC adducts in different solvents

Preparation

Dispersions of HSAG-PyC adducts were prepared at different concentrations: 1 mg/mL; 0.5 mg/mL; 0.3 mg/mL; 0.1 mg/mL. Each dispersion was sonicated for 30 min using an ultrasonic bath (260 W) and subsequently UV-Vis absorption was measured. The dispersion (10 mL) of each sample was put in a Falcon™ 15 mL conical centrifuge tubes and centrifuged at 6000 rpm for 30 min. UV-Vis absorptions were measured immediately after each centrifugation and after 1-week storage.

UV-Vis spectroscopy

Suspension of adduct (3 mL) was placed by pipette Pasteur, in quartz cuvettes of 1 cm optical path (volume 1 or 3 mL) and analyzed by a Hewlett Packard 8452A diode array spectrophotometer, firstly resetting the instrument with the pure solvent (as background) and then acquiring the UV spectrum from 200 to 900 nm. The UV-visible spectrum reported intensity the absorption as a function of the wavelength of the radiation between 200 and 750 nm.

Calculation of the Hansen solubility sphere and Hansen solubility parameters

The calculation of the Hansen solubility parameters (HSP) for HSAG was performed applying the Hansen solubility sphere representation of miscibility. The idea at the basis of this geometrical approach is the calculation of the cohesive energy density (U_T/V) of a compound as the sum of three interaction contributions, as given by eq. 2: dispersion (non-polar van der Waals forces) (δ_D), polar (δ_P), and hydrogen bonding (δ_H).

$$\frac{U_T}{V} = \delta_T^2 = \delta_D^2 + \delta_P^2 + \delta_H^2 \tag{2}$$

The compound is therefore identified by three coordinates (δ_D, δ_P and δ_H) in the Hansen parameters space. The distance between two points (e.g. a solute and its solvent) is related to their cohesive energy density difference, which is related to the enthalpy of mixing. As the enthalpy of mixing is minimal for miscible substances, two point close to each other in the Hansen space correspond to miscible compounds.

To estimate the HSP of a solute *i*, a dispersion test is performed on different solvents *j*, distinguishing good solvents (providing stable solutions/dispersions) and bad solvents, which are not able to give stable dispersions. Given the parameters (coordinates) of the solvents, it is possible to define a sphere, centered on the solubility parameters of the solute, which encompasses the good solvents points and excludes the non-solvents. The sphere radius is defined as R_o, the radius of interaction, while the distance between the solute and the solvent is R_a, calculated as in eq. 3.

$$R_{a,ij}{}^2 = 4(\delta_{D,i} - \delta_{D,j})^2 + (\delta_{P,i} - \delta_{P,j})^2 + (\delta_{H,i} - \delta_{H,j})^2 \tag{3}$$

The ratio between $R_{a,ij}$ and R_0 is defined in eq. 4 as RED, relative energy difference. Solutes and solvents with good affinity have relative energy difference lower than 1 [55].

$$\mathrm{RED} = \frac{R_{a,ij}}{R_o} \tag{4}$$

An optimization problem is therefore defined: the center coordinates of the Hansen solubility sphere are calculated by minimizing the radius of interaction (i.e. the distance from the coordinates of the good solvents), including the good solvents (RED < 1) and excluding the bad ones. The sphere center coordinates correspond to the three unknown HSP of the solute.

The fitting sphere program was adapted from [60] and solved in Matlab environment using the Nelder-Mead simplex algorithm.

Results and discussion

Pyrrole based compounds were prepared through the Paal–Knorr reaction [37, 38], by reacting a primary amine with 2,5-HD, as schematically shown in Fig. 1.

The structures of primary amines used for the reactions and of pyrrole compounds obtained therefrom are shown in Table 1.

All the reactions of Table 1 are characterized by very good atom economy (from 81 % to 90 %), the only byproduct being water, and all the syntheses were carried out in the absence of solvents and catalyst [51, 52, 61]. Detailed procedures are reported in the experimental part. In brief, neat reactions were carried out in temperatures' range from 130 °C to 150 °C for 3 h. Some of the authors reported the preparation of 2-(2,5-dimethyl-1*H*-pyrrol-1-yl)-1,3-propanediol from 2-amino-1,3-propandiol (also known as serinol) as the primary amine [21, 51, 52] and such preparation has been reproduced in the present work with a yield of 96 % and with an atom economy (AE) of 83 % and a reaction mass efficiency (RME) of 80 %. Most of the reaction of Table 1, with primary amine other than serinol, had a yield of at least 70 % and some of them of at least 80 %. The pyrrole compounds of Table 1 were thus obtained with a process that can be defined "sustainable", characterized by reaction mass efficiency from 55 % to 80 %. Mechanistic implications, not reported in this manuscript, will be discussed in a forthcoming paper.

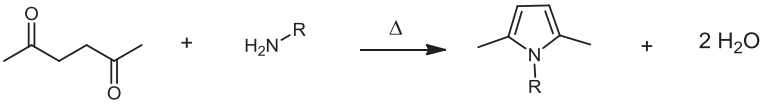

Fig. 1: Synthesis of pyrrole based compounds.

Table 1: Reactions of 2,5-hexanedione with different primary amines.

Amine	Time (h)	T (°C)	Yield (%)	AE[a,c] (%)	RME[b,c] (%)	Acronym	Product
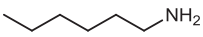	3	130	73	84	62	HP	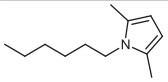
	3	130	62	88	55	DDcP	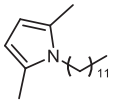
	3	130	73	90	66	ODcP	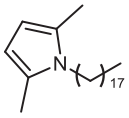
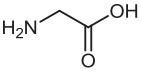	3	130	80	81	65	GlyP	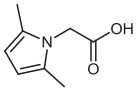
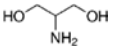	3	150	96	83	80	SP	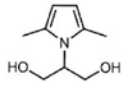
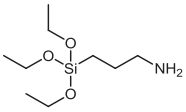	3	130	80	89	71	APTESP	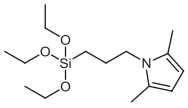

[a]AE, Atom economy; [b]RME, reaction mass efficiency; [c]for explanation see the Experimental part.

Thanks to the reactions of Table 1, a library of pyrrole based compounds became available. These compounds were used for the functionalization of graphene layers.

As reported in the introduction, SP has been shown able to form stable adducts with graphitic substrates [20–22, 62]. It was commented [21, 22] that SP is a *Janus* molecule, that is a molecule with two faces. Such a definition, which comes from the Roman god Janus, has been used in the scientific literature to indicate particles with at least two physically or chemically different surfaces [63, 64] and molecules with two moieties, typically one hydrophobic and the other hydrophilic, as in the case of colloids [65] and block copolymers [66]. SP was used to functionalize sp^2 carbon allotrope [20–22, 62] relying on the interaction of the pyrrole ring the with aromatic substrate. Indeed, the Paal Knorr reaction changes the hybridization of the nitrogen atom, from sp^3 in the amino group, to sp^2 in the aromatic pyrrole ring. This could promote the π-π stacking with aromatic compounds such as graphene layers. Stable adducts were prepared and hence sustainable oxidation of the carbon allotropes was achieved [20, 22], in particular of graphene layers [21]. Stable dispersions of adducts of carbon allotropes with SP were prepared, both in water and polar environments [20–22, 62].

In this work, functionalization reactions of HSAG with the pyrrole compounds of Table 1 were performed to prepare HSAG-PyC adducts. The experimental frame already used for preparing HSAG-SP adducts was adopted [20–22]. The HSAG/PyC molar ratio (considering the moles of C6 rings as the moles of the graphitic substrate) was 10:1 and thermal energy was used to favor the formation of the adduct. The optimization of the reaction conditions, as a function of the pyrrole compound, was not performed. The experiments with PyC other than the serinol based one should be thus considered as preliminar. Details of the reactions are in the experimental part and the process is schematically shown in the block diagram in Fig. 2. In brief, HSAG and the selected pyrrole compound were mixed and the HSAG/PyC mixture was then heated in a flask for 2 h at 180 °C.

Fig. 2: Block diagram for the preparation of HSAG-PyC adducts with the help of thermal energy.

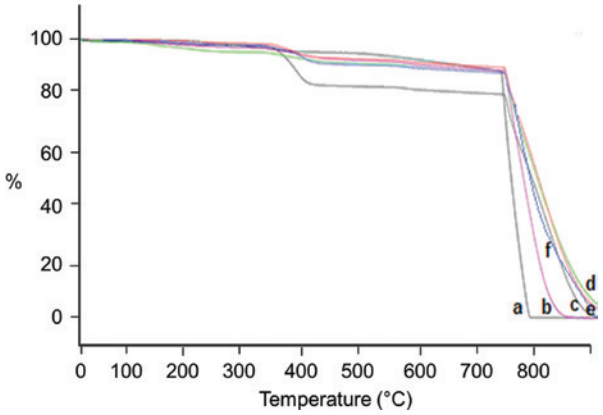

Fig. 3: TGA curves of HSAG (a, black), HSAG-HP (b, purple) and HSAG-DDcP (c, brown) HSAG-Gly (d, red), HSAG-APTESP (e, green) and HSAG-SP (f, blue).

Table 2: Mass loss for HSAG, HSAG-PyC adducts, from TGA analysis.

Sample		Mass loss (%)			
		T < 150 °C	150 °C < T < 400 °C	400 °C < T < 700 °C	T > 700 °C
HSAG	(a)	1.3	1.7	4.6	92.4
	(b)	0.0	0.1	0.4	99.5
HSAG-DDcP	(a)	0.0	4.0	22.4	73.6
	(b)	0.0	4.0	15.4	80.6
HSAG-Gly	(a)	1.0	6.9	10.9	81.2
	(b)	1.0	4.1	7.0	87.9
HSAG-SP	(a)	1.0	6	9.4	83.6
	(b)	1.0	5	8.5	85.5

(a) After reaction (b) after washing with acetone (see Experimental part).

Although the optimization of the reaction conditions for the preparation of HSAG/PyC adducts was not performed, the efficiency of the functionalization reaction was investigated on some adducts: the HSAG/PyC powder taken from the flask was extracted in Soxhlet with acetone, until PyC was undetectable in the washing acetone (GC-MS was performed on washing acetone).

Thermogravimetric analysis was performed on HSAG and HSAG-PyC samples, before and after extraction with acetone. TGA, as explained in detail in the experimental part, was performed under nitrogen on HSAG and on the HSAG-PyC adducts. Thermographs are shown in Fig. 3. Data are in Table 2.

The decomposition profile for all the samples, HSAG and HSAG/PyC adducts, reveals three main steps, in the following temperature ranges: below 150 °C, from 150 °C to 700 °C and above 700 °C. Mass loss at T < 150 °C could be due to absorbed low molar mass substances, mainly water. Mass loss in the temperature range from 150 °C to 700 °C could be attributed to decomposition of PyC compounds and also of alkenylic groups, present as defects in HSAG. Combustion with oxygen occurs at T > 700 °C.

A small mass loss (0.5 %) was detected for HSAG washed with acetone in the temperature range between 150 °C and 700 °C and was attributed, as mentioned before, to the alkenylic defects. Mass loss in pristine HSAG sample could be due to impurities (whose nature was not investigated) coming from the process and also from the packaging. As written in the experimental part, all reactions with PyC were performed on washed samples. The amount of PyC in the adduct was estimated evaluating the mass loss in the temperature range from 150 °C to 700 °C and comparing data before and after washing. The values of mass loss of HSAG-PyC adducts before acetone extraction, shown in Table 2, are substantially in line, as expected, with the theoretical values of % of PyC in the HSAG-PyC mixture, before the reaction (reported in the experimental part). HSAG-PyC adducts based on polar PyC show larger mass loss below 150 °C and this could be due

to larger amount of absorbed water. The mass loss of HSAG-PyC adducts, after washing with acetone, in the temperature range from 150 °C to 400 °C, is indeed appreciable. This finding indicates the formation of stable HSAG-PyC adducts. Equation for calculating the functionalization yield and yield data for all the HSAG-PyC adducts are reported in the experimental part. Larger functionalization yield, 87 %, was obtained with SP as the pyrrole compound. The yield was about 73 % for PyC based on DDcP as primary amine, almost 70 % for PyC based on APTES as the primary amine and was about 61 % with Gly as the PyC. At the present state of the research, it is not possible to speculate on such differences. To account for them, to explain the detection in IR spectra of functional groups not present in PyC and, most of all, to justify the formation of stable HSAG-PyC adducts, a mechanism for adducts formation should be clarified.

The strong interaction between PyC and the graphitic substrate has been preliminary attributed to the π-π interaction between the aromatic moieties, the C6 rings in the graphene layers and the pyrrole ring in SP [21, 22]. However, further experimental findings [67] seem to suggest that domino reactions occur: the pyrrole compound undergoes to oxidation, mainly in two position, in the presence of air and thanks to the catalytic activity of carbon substrate. Such oxidated products, which could explain the presence of carbonylic compounds in IR spectra, could act as dienophile in cycloaddition reaction with dienes of the graphene layers. More experiments and DFT calculations are in progress to further investigate and, in case, validate this hypothesis. Indeed, this work has not the objective to stretch too far such inferences, though intriguing, on the mechanism for HSAG-PyC adducts formation but rather to present and discuss experimental data.

The vibrational characterization of pristine HSAG and HSAG-PyC adducts (after acetone extraction) was performed through Raman and IR spectroscopies. Main objective of Raman analysis was to characterize the bulk structure of the graphitic materials before and after the reaction for the adducts' formation. IR analysis was mainly intended to assess the nature of functional groups present on the adducts. The chemical complexity of the samples hampers a straightforward and precise assignment of the spectroscopic signals. Hence, vibrational analysis was based on spectroscopic correlations tools [68].

Raman spectroscopy is widely employed for the study of carbonaceous materials [69–77]. The Raman spectra of HSAG, HSAG-SP, HSAG-Gly, HSAG-HP, HSAG-DDcP, and HSAG-APTESP recorded with the laser excitation at 632.8 nm, are reported in Fig. 4.

The presence of graphitic sp^2-phase in the Raman spectra is principally revealed by two main peaks located at 1580 cm^{-1} and 1350 cm^{-1} named G and D, respectively. The G peak is characteristic of the vibration of bulk crystalline graphite (graphene). On the other hand, the D peak, whose frequency and relative intensity with respect of the G peak depend on the laser excitation wavelength [78], appears in the presence of either structural disorder or confinement effects (e.g. by edges) of the graphitic layers [73–79]. Usually the

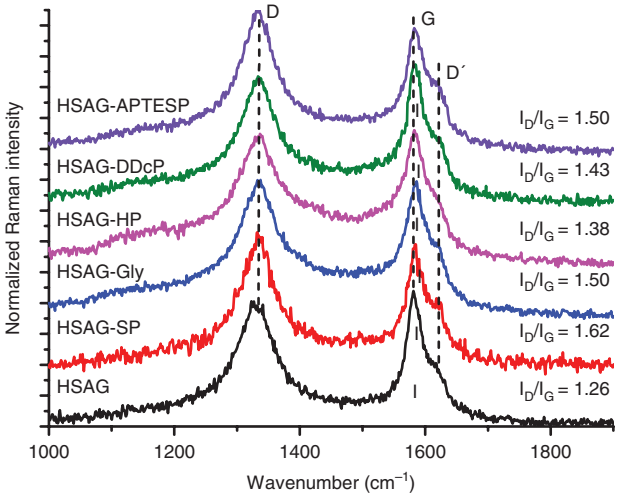

Fig. 4: Raman spectra of HSAG (black), HSAG-SP (red), HSAG-Gly (blue), HSAG-HP (cyan), HSAG-DDcP (green) and HSAG-APTESP (violet) recorded at 632.8 nm; I_D/I_G values are reported. Spectra are displayed with normalized intensity.

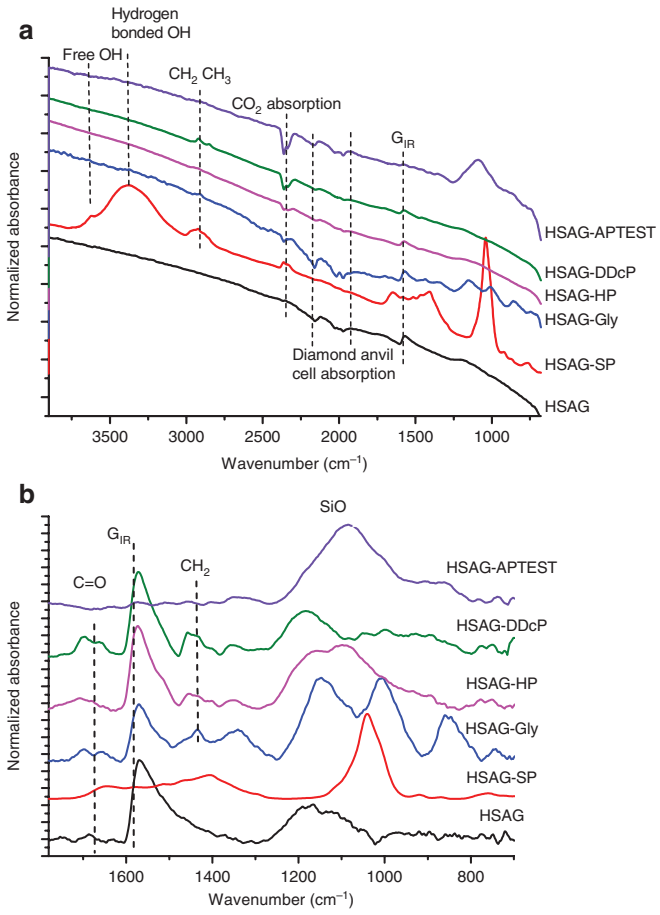

Fig. 5: FTIR spectra of HSAG (black), HSAG-SP (red), HSAG-Gly (blue), HSAG-HP (cyan), HSAG-DDcP (green), and HSAG-APTESP (violet). (a) in the 700–3900 cm^{-1} region, (b) after baseline correction in the fingerprint region 700–1800 cm^{-1}. Spectra are displayed with normalized intensity. CO_2 absorption and DAC artifacts are labeled.

appearance of D peak is accompanied by a D′ peak located near 1620 cm^{-1}. Structural defects can be holes in the graphene layer, sp^3 or sp carbon atoms, dangling bonds, distortions from planarity and grafted functional groups [80].

In the spectrum of the graphitic starting materials (HSAG), the comparable intensity of D and G bands with an I_D/I_G value of 1.26, can be associated to its turbostratic structure with high crystalline order inside the structural layers and a relatively low number of stacked layers [53]. The Raman spectra of different HSAG adducts show a similar pattern with the G peak at 1582 cm^{-1} and evident D and D′ peaks at 1333 cm^{-1} and 1620 cm^{-1}, respectively, accompanied by a weak and very broad component between G and D peaks, associated to the presence of disordered sp^3 carbon structures [70]. Although the spectral pattern of HSAG and HSAG/PyC adducts are quite similar, a small but measurable increase of the ID/IG ratio for the adducts can be observed (see Fig. 4). Such increase is indeed compatible with the occurrence of functional groups (as will be detected in their IR spectra) attached to the graphitic platelets thus reducing the sp^2 domains size and increasing distortion of the edges [80].

The largest value observed in the case of HSAG-SP adduct could be explained with the larger number of functional groups, as supported by experimental data shown below in the text. On the basis of Raman findings, the reaction of HSAG with PyC does not appreciably alter per se the structure of the graphitic layers. As a consequence, it can be assumed that PyC are preferentially located in peripheral positions of the layers.

FT-IR spectra of HSAG and HSAG-PyC adducts, shown in Fig. 5, were used to obtain information on the chemical nature of functional groups present on the graphene layers. In Fig. 5a, spectra are reported in the

700 cm^{-1}–3900 cm^{-1} regions. In Fig. 5b, spectra are shown in the 700 cm^{-1}–1800 cm^{-1} fingerprint region, after baseline correction, in order to enhance the weak spectroscopic features of functional groups.

In Fig. 5a and b, the IR spectra of HSAG, HSAG-HP, HSAG-DDcP and HSAG-Gly are characterized by a common strong feature at 1590 cm^{-1}, assigned to E_{1u} IR active mode of the collective C=C stretching vibration (G_{IR}) of graphitic materials. Viceversa, the spectra of HSAG-SP and HSAG-APTESP are both dominated by the very strong absorptions characteristic of their functional groups, which shadow the signal from the graphitic moieties of the adducts. Therefore, the G_{IR} bands of of HSAG-SP and HSAG-APTESP, although present, are hardly observable.

For HSAG-HP and HSAG-DDcP, the bands near 2900 cm^{-1} (assigned to CH stretching vibrations of CH_3 and CH_2 units) and the bands close to 1450 cm^{-1} (assigned to bending vibrations of CH_3 and CH_2) are clearly visible and reveal the presence of the alkyl residues present in PyCs. With respect to these spectra, the spectrum of HSAG-Gly shows different and less intense CH stretching pattern near 2900 cm^{-1} and new strong and broad bands at 855 cm^{-1} and 1005 cm^{-1}, which could be tentatively assigned to aliphatic ether. These signals are compatible with the structure of glycine. The spectrum of HSAG-APTESP shows the very strong absorption close 1100 cm^{-1}, which is typical of SiO stretching vibration. Also in this case the spectrum is compatible with the chemical nature of the functional group in PyC. The spectrum of HSAG-SP differs from the previous cases and it is dominated by (i) the very strong absorptions near 3400 cm^{-1} and 1040 cm^{-1}, respectively assigned to the stretching of hydrogen bonded OH groups and to the stretching of C–O–R groups and by (ii) the strong and broad bands at 1650 cm^{-1} and 1400 cm^{-1} assigned to the C=C stretching of the pyrrole ring. All these vibrations are compatible with the presence of SP functionalities in the adduct. These findings from IR analysis, performed on samples thoroughly washed with acetone, support the formation of HSAG-PyC adducts. Particularly remarkable was the presence of other absorptions, common to all the samples. These can be observed at the following wavelengths: close to 1700 cm^{-1}, suggesting the presence of carbonylic C=O stretching vibrations and in the 1100–1200 cm^{-1} range, compatible with the stretching vibrations of C–O–C and C–OH functional groups. These functional groups should not be present, on the basis of PyC structure. To account for their presence, some further insight can derive from the hypothesis of the formation mechanism of HSAG-PyC adduct, presented below in the text.

Dispersions of HSAG-PyC adducts of Table 2 were prepared in solvents having different solubility parameter: water, isopropanol, ethyl acetate, n-heptane, toluene. The stability of the dispersions was studied, as described in the experimental part. In brief, dispersions were first sonicated, stored for 1 week at rest and then centrifuged and UV-Vis absorption was measured before and after such treatments.

The structure of HSAG-PyC adducts was investigated by performing HR-TEM analysis on samples isolated from the supernatant suspensions, before and after centrifugation for 30 min at 6000 rpm (c, d). Figure 6 shows HR-TEM micrographs of HSAG-DDcP adduct, before (a, b) and after (c, d) centrifugation, at lower (a, c) and at higher magnifications (b, d).

Micrographs at lower magnification in Fig. 6a and c reveal that the lateral size of HSAG-DDcP adducts is of the same order of magnitude in samples isolated before and after centrifugation at 6000 rpm for 30 min. This indicates that the heating step for the preparation of the adduct (and also sonication) does not cause appreciable breaking of the graphitic layers. Micrographs at higher magnification allow to visualize the stacks of graphene layers that are disposed with a lateral side perpendicular to the beam. Thanks to this disposition of the nano-stacks, it is possible to estimate the number of stacked graphene layers. Figure 6b shows stacks isolated after centrifugation for 30 min at 6000 rpm: stacks made by about 2–3 stacked graphene layers are visible (indicated in the box). As revealed by the exam of a good number of micrographs, such stacks are the most abundant ones in a population of stacks that also contain little larger number of layers.

As reported in the Introduction, the objective of studying the dispersion of HSAG-PyC adducts in different solvents was to investigate the ability of PyC to modify the solubility parameter of graphene layers. The solubility parameters indicate the degree of interaction between materials. As mentioned in the Introduction, matching the solubility parameter of a carbon nanomaterial with the neighboring materials is the prerequisite to favor separation of the nanomaterial into individual particles [54] and to achieve ultimate dispersion in a polymer

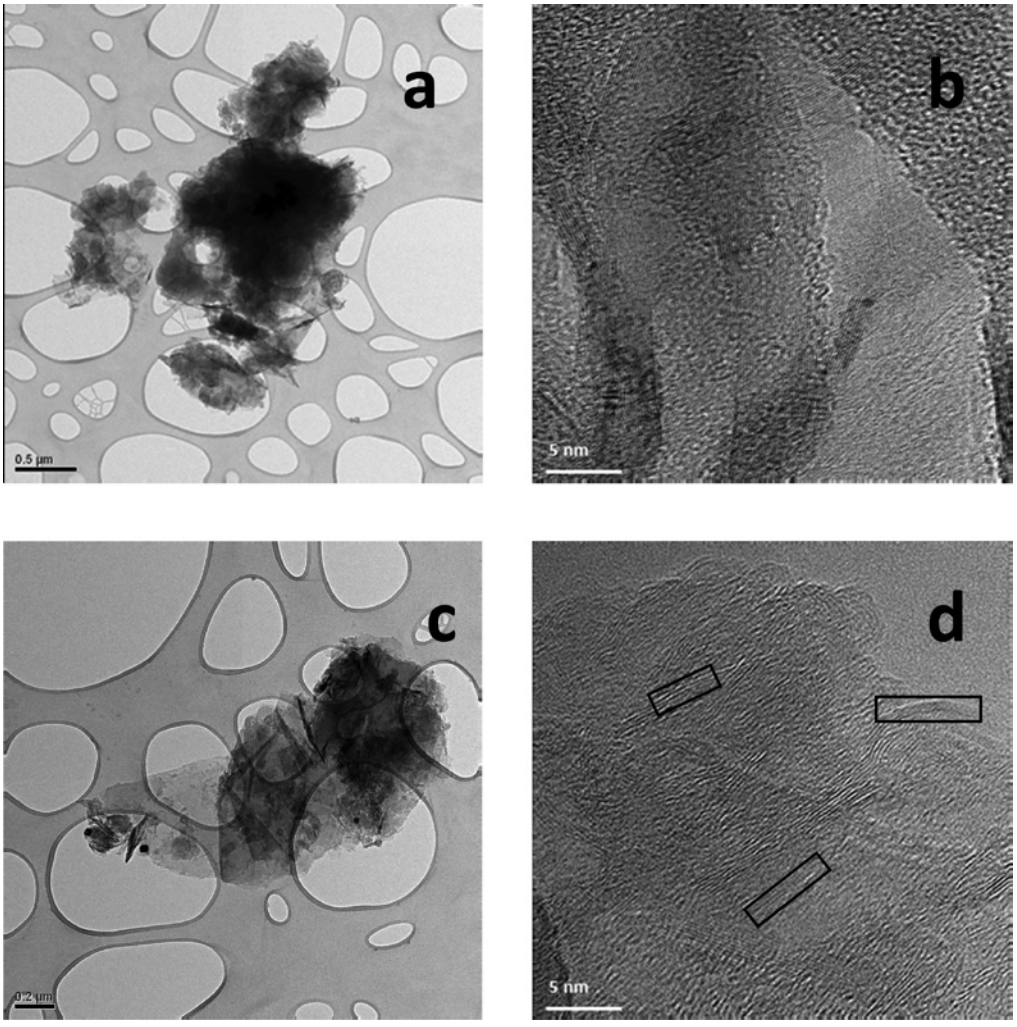

Fig. 6: Micrographs of HSAG-DDcP adduct isolated from supernatant solutions before and after centrifugation for 30 min at 6000 rpm (a, b). Micrographs are: low magnification bright field TEM (a, c), HRTEM images (b, d).

matrix [57]. In this work, the dispersion of HSAG-PyC adduct in a solvent was inspected upon sonication and, in case of homogeneous dispersion (HSAG-PyC did not settle down or float on the solvent), was monitored also after 1 week storage at rest. In Table 3, the inspections of HSAG-PyC adducts' dispersions in the different solvents are summarized: 'good' indicates that a homogenous dispersion was observed, immediately after sonication and also after 1 week, 'bad' indicates the separation of the adduct from the solvent.

An example of a stable dispersion, of HSAG-DDcP adduct (1 mg/mL) in ethyl acetate, is shown in Fig. 7.

UV-Vis absorption analysis was performed on dispersions of HSAG-PyC adducts with 0.001, 0.1, 0.25, 0.5, 0.75 and 1 mg/mL as adduct concentration. In Fig. 8, are shown UV-Vis spectra of HSAG-DDcP adduct in n-heptane. Graph in Fig. 8a clearly shows that the absorbance, taken immediately after sonication, monotonously increases with the adduct concentration. The stability of the dispersion, with 1 mg/mL as the adduct concentration, was investigated by taking UV-Vis spectra on samples stored for 1 week and on samples centrifuged at 6000 rpm for 30 min. In Fig. 8b, the absorbance of the dispersion stored for 1 week appears to be slightly lower than the absorbance of the freshly prepared dispersion. The absorbance of the dispersion centrifuged at 6000 rpm is appreciably lower, remaining however at a remarkable level.

The amount of adduct left in the suspension after 1 week storage and after centrifugation were estimated with the help of the calibration curve of Fig. 8a, by deriving the equation of the calibration curve:

Table 3: Results of inspection of dispersions of HSAG-PyC adducts in various solvents.[a,b]

Adduct	Solvents				
	Water	Isopropanol	Ethyl acetate	Toluene	Heptane
HSAG-SP	Good	Good	Good	Bad (↓)	Bad (↓)
HSAG-Gly	Bad (↓)	Good	Good	Good	Bad (↓)
HSAG-APTESP	Bad (↑)	Bad (↓)	Bad (↓)	Good	Good
HSAG-TMP	Bad (↓)	Good	Good	Good	Good
HSAG-HP	Bad (↑)	Bad (↓)	Good	Bad (↓)	Good
HSAG-DDcP	Bad (↑)	Good	Good	Bad (↓)	Bad (↓)

[a]Concentration: 1 mg/mL; [b]good: homogenous dispersion was observed soon after sonication and after 1 week storage at rest; bad: separation of adduct from the solvent: the adduct floated on the solvent (upward arrow), or settled down (downward arrow).

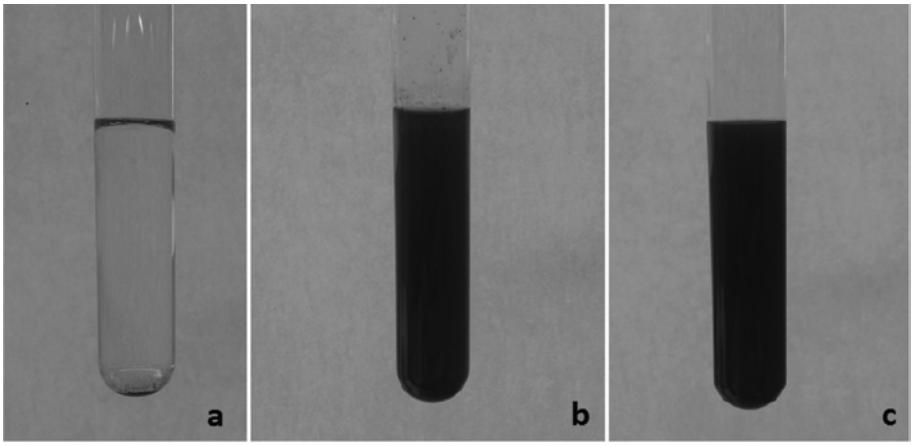

Fig. 7: Dispersions in ethyl acetate of pristine HSAG (a) and HSAG-DDcP adduct (1 mg/mL) freshly prepared (b) and after 1 week storage (c).

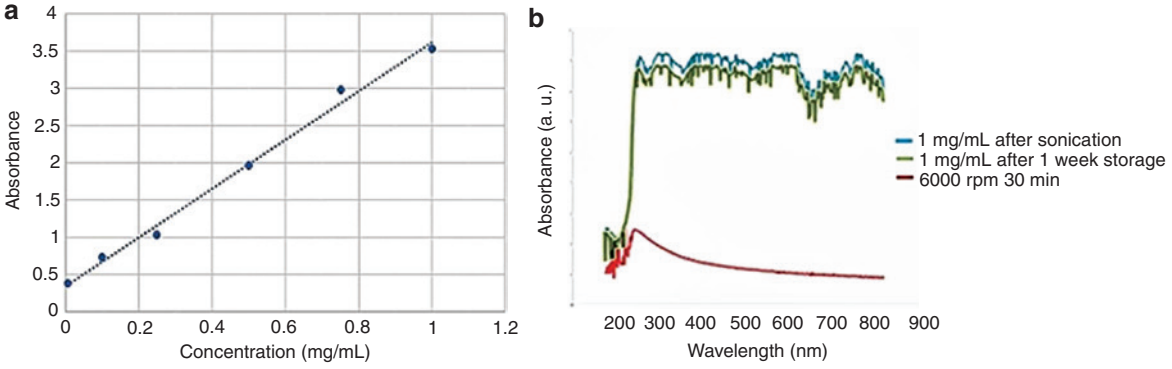

Fig. 8: (a) Linear relationship between the absorbance at 300 nm and the concentration of HSAG-DDcP adduct in heptane; (b) UV-Vis traces of the same sample after sonication, 1 week storage and centrifugation.

$y = 3.2759x + 0.3524$ ($R^2 = 0.992$). On the basis of the absorbance of the dispersions (3.53 and 0.52 a.u.), concentrations were 1 mg/mL and 0.05 mg/mL, respectively.

The HSAG-DDcP adduct was considered for the estimation of its Hansen solubility parameter. For this study, eight solvents, listed in Table 4 with their Hansen solubility parameters, were used. Stability of dispersions was inspected after 3 weeks storage, classifying the solvents as good or bad, as explained above, by inspecting the dispersions after 3 weeks.

Table 4: Hansen solubility parameters for selected solvents and affinity with HSAG-DDcP adduct after 3 weeks.

Solvent	δ_D [MPa$^{1/2}$]	δ_P [MPa$^{1/2}$]	δ_H [MPa$^{1/2}$]	Affinity
2-Butanol	15.8	5.7	14.5	Good
2-Propanol	15.8	6.1	16.4	Good
Water	15.5	16.0	18.6	Bad
Ethyl acetate	15.8	5.3	7.2	Good
Heptane	15.3	0	0	Bad
Methanol	15.1	12.3	22.2	Bad
THF	16.8	5.7	8	Good
Xylene	17.6	1	3.1	Bad

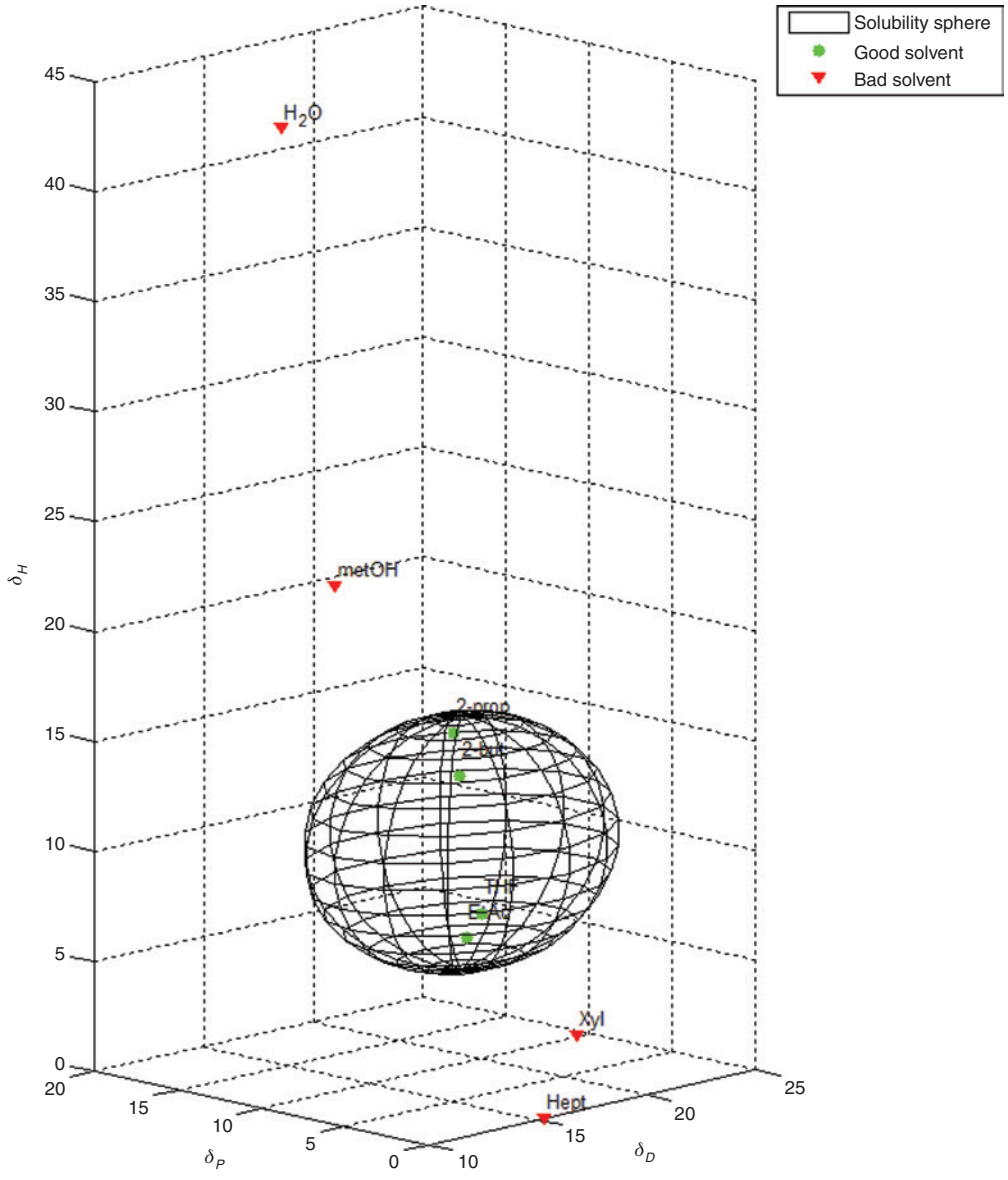

Fig. 9: Hansen solubility sphere calculated for HSAG-DDcP. The calculated HSP are δ_D 16.5 MPa$^{0.5}$, δ_P 6.6 MPa$^{0.5}$ and δ_H 11.2 MPa$^{0.5}$. The green circles correspond to the good solvents (within the radius of interaction), the red triangles to the bad solvents (outside the sphere).

Heptane was classified as a "bad" solvent, as sedimentation was observed after 1 week, as commented above. Still, a solvent such as heptane can be useful for preparing HSAG adducts dispersions in virtue of its volatility, or to perform short time analyses.

The qualitative "good" or "bad" classification of Table 4 was used to identify the unknown Hansen Solubility Parameters of HSAG-DDcP, applying a fitting sphere algorithm. The sphere shown in Fig. 9 was generated, as explained in the experimental part, to encompass the good solvents points and to exclude the bad solvent, being centered on the solubility parameters of the HSAG-DDcP adduct. Solubility parameters of the adduct δ_D, δ_P and δ_H values were estimated to be 16.5 $MPa^{0.5}$, 6.6 $MPa^{0.5}$, 11.2 $MPa^{0.5}$, respectively, while the solubility radius was found to be 5.8. Hence, polar aprotic solvents such as THF and ethyl acetate are well within the sphere and also polar protic solvents such as 2-butanol and 2-propanol are included in the HSAG-DDcP interaction sphere. These results indicate that the contribution of polar interaction and hydrogen-bonding is appreciable, also in an adduct which should be considered apolar. This is probably due to the presence of oxygenated groups in alfa position of the pyrrole ring. Values of solubility parameters of graphene have been reported in the literature [56]: δ_D 18 $MPa^{0.5}$, δ_P 9.3 $MPa^{0.5}$ and δ_H 7.7 $MPa^{0.5}$. It appears that the importance of the hydrogen-bonding contribution is larger in HSAG-DDcP adduct.

Even though these results are indeed preliminary (the quality of the regression could be improved by using more solvents) these HSP estimates can be used to predictively identify the materials with the highest affinity (RED < 1), among the thousands of compounds in the Hansen database.

Conclusions

Graphene layers were functionalized with pyrrole compounds obtained by means of the Paal–Knorr reaction of a primary amine with 2,5-hexanedione. PyC were prepared with a variety of primary amines, from hexanamine to octanamine, from 2-aminoacetic acid to 2-amino-1,3-propanediol to 3-(triethoxysilyl)propan-1-amine. Neat reactions were performed in the absence of any catalyst and were characterized by high yields: the average value was 77 %, whereas the largest yields were 80 % and 91 % for PyC from 3-(triethoxysilyl)propan-1-amine and 2-amino-1,3-propanediol. Adducts of PyC with a high surface area graphite were prepared by simply mixing and providing thermal energy, heating for 3 h at 180 °C. FT-IR analysis clearly revealed the presence of functional groups coming from PyC and Raman spectra showed the substantially unaltered structure of the graphitic substrate after the reaction. Stable dispersions of HSAG-PyC adducts, based on different PyC, were obtained in solvents with different solubility parameters. Experimental qualitative data were used to calculate the Hansen solubility parameter of HSAG adduct with DDcP.

This work demonstrates that graphene layers can be functionalized with a facile and sustainable reaction, obtaining the modification of their solubility parameters. These parameters allow to predictively assess the compatibility between the adduct and an increased number of neighbor materials, such as solvents and polymers. Also, the parameters can give a further theoretical insight on the nature of the involved molecular interactions. The results of this work could possibly accelerate a large-scale application of nanosized graphitic materials.

Acknowledgements: Authors gratefully acknowledge Dr. Andrea Serafini (Politecnico di Milano) for HRTEM micrographs.

References

[1] K. Novoselov, A. K. Geim, S. V. Morozov, D. Jiang, Y. Zhang, S. V. Dubonos. *Science* **306**, 666 (2004).
[2] A. K. Geim, A. H. MacDonald. *Phys. Today* **60**, 35 (2007).
[3] R. F. Service. *Science* **324**, 875 (2009).
[4] A. K. Geim, K. S. Novoselov. *Nat. Mater.* **6**, 183 (2007).

[5] K. S. Novoselov, A. K. Geim, S. V. Morozov, D. Jiang, M. I. Katsnelson, I. V. Grigorieva, S. V. Dubonos, A. A. Firsov. *Nature* **438**, 197 (2005).
[6] M. D. Stoller, S. Park, Y. Zhu, J. An, R. S. Ruoff. *Nano Lett.* **8**, 3498 (2008).
[7] S. Chen, Q. Wu, C. Mishra, J. Kang, H. Zhang, K. Cho, W. Cai, A. A. Balandin, R. S. Ruoff. *Nat. Mater.* **11**, 203 (2012).
[8] C. Soldano, A. Mahmood, E. Dujardin. *Carbon* **48**, 2127 (2010).
[9] H. Greenberg, U. Jansson. "Advanced functional materials", in *Science and Technology of Atomic, Molecular, Condensed Matter & Biological Systems,* Tara Prasad Das (Ed.), Vol. 2, pp. 1–238, Elsevier B.V., Toronto (2012).
[10] Y. Hernandez, S. Pang, X. Feng, K. Müllen. *Pol. Sci.: A Comprehensive Reference* **8**, 415 (2012).
[11] S. Eigler, S. Grimm, F. Hof, A. Hirsch. *J. Mater. Chem. A* **1**, 11559 (2013).
[12] E. P. Randviir, D. A. C. Brownson, C. E. Banks. *Mater. Today* **17**, 426 (2014).
[13] H. Yang, F. Li, C. Shan, D. Han, Q. Zhang, L. Niu, A. Ivaskab. *J. Mater. Chem.* **19**, 4632 (2009).
[14] T. M. Swager. *ACS Macro Lett.* **1**, 3 (2012).
[15] I. Zaman, H.-C. Kuan, Q. Meng, A. Michelmore, N. Kawashima, T. Pitt, L. Zhang, S. Gouda, L. Luong, J. Ma. *Adv. Funct. Mater*. **22**, 2735 (2012).
[16] C. K. Chua, M. Pumera. *Chem. Soc. Rev.* **42**, 3222 (2013).
[17] D. Bhattacharjya, I. Y. Jeon, H. Y. Park, T. Panja, J. Beom Baek, J. S. Yu. *Langmuir* **31**, 5676 (2015).
[18] P. Xiong, J. Zhu, L. Zhang, X. Wang. *Nanoscale Horiz*. **1**, 340 (2016).
[19] A. Kausar, Z. Anwar, L. A. Khan, B. Muhammad. *Fuller. Nanotub. Car. N.* **25**, 47 (2017).
[20] M. Galimberti, V. Barbera, A. Citterio, R. Sebastiano, A. M. Valerio, G. Leonardi WO2015EP72641 (2015).
[21] M. Galimberti, V. Barbera, S. Guerra, L. Conzatti, C. Castiglioni, L. Brambilla, A. Serafini, *RSC Adv.* **5**, 81142 (2015).
[22] M. Galimberti, V. Barbera and A. Sironi. "Controlled functionalization of graphene layers", in *Graphene Materials – Structure, Properties and Modifications*, G. Kyzas (Ed.), InTech, Croatia (2017).
[23] V. Barbera, A. Porta, L. Brambilla, S. Guerra, A. Serafini, A. M. Valerio, M. Galimberti. *RSC Adv.* **6**, 87767 (2016).
[24] V. Singh, D. Joung, L. Zhai, S. Das, S. I. Khondaker, S. Seal. *Progr. Mater. Sci.* **56**, 1178 (2011).
[25] Z. U. Khan, A. Kausar, H. Ullah, A. Badshah, W. U. Khan. *J. Plast. Film Sheet*. **32**, 336 (2016).
[26] V. L. Pushparaj, M. M. Shaijumon, A. Kumar, S. Murugesan, L. Ci, R. Vajtai, R. J. Linhardt, O. Nalamasu, P. M. Ajayan. *Proc. Natl. Acad. Sci. USA* **104**, 13574 (2007).
[27] M. M. Waje, X. Wang, W. Li, Y. Yan. *Nanotechnology* **16**, 395 (2005).
[28] H. Yagoh, H. Murayama, T. Suzuki, Y. Tominaga, N. Shibuya, Y. Masuda. *Anal. Sci.* **22**, 583 (2006).
[29] F. Zheng, D. L. Baldwin, L. S. Fifield, N. C. Anheier Jr, C. L. Aardahl, J. W. Grate. *Anal. Chem.* **78**, 2442 (2006).
[30] J. N. Coleman, W. J. Blau, A. B. Dalton, E. Muñoz, S. Collins, B. G. Kim, J. Razal, M. Selvidge, G. Vieiro, R. H. Baughman. *Appl. Phys. Lett.* **82**, 1682 (2003).
[31] A. Tabasi, A. Noorbakhsh, E. Sharifi. *Biosens. Bioelectron.* **95**, 117 (2017).
[32] P. Yua, R.-Y. Baoa, X.-J. Shib, W. Yanga, M.-B. Yang. *Carbohydr. Polym.* **155**, 507 (2017).
[33] S. Navalon, A. Dhakshinamoorthy, M. Alvaro, H. Garcia. *Chem. Rev.* **114**, 6179 (2014).
[34] C. K. Chua, M. Pumera. *Chem. Eur. J.* **21**, 12550 (2015).
[35] D. R. Dreyer, C. W. Bielawski. *Chem. Sci*. **2**, 1233 (2011).
[36] V. O. Piloty. *Eur. J. Inorg. Chem.* **43**, 489 (1910).
[37] L. Knorr. *Chem. Ber.* **18**, 299 (1885).
[38] C. Paal. *Chem. Ber.* **18**, 367 (1885).
[39] D. H. Barton, J. Kervagoret, S. Z. Zard. *Tetrahedron* **46**, 7587 (1990).
[40] A. Hantzsch. *Ber. Dtsch. Chem. Ges.* **23**, 1474 (1890).
[41] A. V. Gulevich, A. S. Dudnik, N. Chernyak, V. Gevorgyan. *Chem. Rev.* **113**, 3084 (2013).
[42] V. Estevez, M. Villacampa, J. C. Menendez. *Chem. Soc. Rev.* **39**, 4402 (2010).
[43] B. B. Thompson, J. Montgomery. *Org. Lett.* **13**, 3289 (2011).
[44] V. Amarnath, D. C. Anthony, K. Amarnath, W. M. Valentine, L. A. Wetterau, D. G. Graham. *J. Org. Chem.* **56**, 6924 (1991).
[45] H. S. Broadbent, W. S. Burnham, R. M. Sheeley, R. K. Olsen. *J. Heterocycl. Chem*. **13**, 337 (1976).
[46] H. Veisi, R. Azadbakht, M. Ezadifar, S. Hemmati. *J. Heter. Chem.* **50**(S1), (2013).
[47] M. Abid, A. Spaeth, B. Török. *Adv. Synth. Catal*. **348**, 2191 (2006).
[48] G. N. Reddy, P. R. Likhar. *Res. Chem. Intermediat.* **42**, 6873 (2016).
[49] L. Akelis, J. Rousseau, R. Juskenas, J. Dodonova, C. Rousseau, S. Menuel, F. Hapiot. *Eur. J. Org. Chem.* **1**, 31 (2016).
[50] Z. H. Zhang, J. J. Li, T. S. Li. *Ultrason. Sonochem*. **15**, 673 (2008).
[51] V. Barbera, A. Citterio, M. Galimberti, G. Leonardi, R. Sebastiano, S. U. Shisodia, A. M. Valerio WO2015189411 (2015).
[52] M. Galimberti, V. Barbera, A. Citterio, R. Sebastiano, A. Truscello, A. M. Valerio, L. Conzatti, R. Mendichi. *Polymer* **63**, 62 (2015).
[53] M. Mauro, V. Cipolletti, M. Galimberti, P. Longo, G. Guerra. *J. Phys. Chem. C* **116**, 24809 (2012).
[54] S. D. Bergin, Y. Hernandez, M. Lotya, D. Rickard, S. D. Bergin, J. N. Coleman. *ACS Nano.* **3**, 2340 (2009).
[55] H. Launay, M. H. Charles, A. Kristoffer. *Carbon* **45**, 2859 (2007).
[56] Y. Hernandez, M. Lotya, D. Rickard, S. D. Bergin, J. N. Coleman. *Langmuir* **26**, 3208 (2010).
[57] S. Ata, T. Mizuno, A. Nishizawa, C. Subramaniam, D. N. Futaba, K. Hata. *Sci. Rep*. **4**, 7232 (2014).

[58] C. M. Hansen. *Hansen Solubility Parameters: A User's Handbook*, 2nd ed. CRC Press, Boca Raton, Florida (2007).
[59] D. J. Constable, A. D. Curzons, V. L. Cunningham. *Green Chem.* **4**, 521 (2002).
[60] D. L. Olynick, P. D. Ashby, M. D. Lewis, T. Jen, H. Lu, J. A. Liddle, W. Chao. *J. Polym. Sci. Part B Polym. Phys* **47**, 2091 (2009).
[61] M. Galimberti, V. Barbera. Italian patent application, n. 102016000113012, Nov 2016.
[62] M. Galimberti, V. Barbera, S. Guerra, A. Bernardi. *Rubber Chem. Technol.* **90**, 285 (2017).
[63] C. Casagrande, P. Fabre, M. Veyssie, E. Raphael. *Europhys. Lett.* **9**, 251 (1989).
[64] P. G. De Gennes. *Angew. Chem. Int. Ed.* **31**, 842 (1992).
[65] F. Li, D. P. Josephson, A. Stein. *Angew. Chem. Int. Ed.* **50**, 360 (2011).
[66] H. Mori, A. H. Müller. *Progr. Polym. Sci.* **28**, 1403 (2003).
[67] V. Barbera, A. Milani, L. Brambilla, C. Castiglioni, M. Galimberti. "VII Workshop Nazionale AICIng, Milano, 12–13 Giugno 2017" Eds Edises ISBN 978–88–6584–960–3.
[68] G. Socrates. *Infrared Characteristic Group Frequencies*. 2nd ed. Wiley, New York (1980).
[69] A. C. Ferrari, J. C. Meyer, V. Scardaci, C. Casiraghi, M. Lazzeri, F. Mauri, A. K. Geim. *Phys. Rev. Lett.* **97**, 187401 (2006).
[70] A. C. Ferrari. *Solid State Commun.* **143**, 47 (2007).
[71] S. Reich, C. Thomsen. *Philos. Trans. R. Soc.* **362**, 2271 (2004).
[72] M. A. Pimenta, G. Dresselhaus, M. S. Dresselhaus, L. G. Cancado, A. Jorio, R. Saito. *Phys. Chem. Chem. Phys.* **9**, 1276 (2007).
[73] C. Castiglioni, M. Tommasini, G. Zerbi. *Philos. Trans. R. Soc.* A **362**, 2425 **(**2004).
[74] M. Tommasini, E. Di Donato, C. Castiglioni, G. Zerbi, N. Severin, T. Böhme, J. P. Rabe. *AIP Conf. Proc.* **723**, 334 (2004).
[75] D. Graf, F. Molitor, K. Ensslin, C. Stampfer, A. Jungen, C. Hierold, L. Wirtz. *Nano Lett.* **7**, 238 (2007).
[76] C. Casiraghi, A. Hartschuh, H. Qian, S. Piscanec, C. Georgi, A. Fasoli, A. C. Ferrari. *Nano Lett.* **9**, 1433 (2009).
[77] L. R. Radovic, B. Bockrath. *J. Am. Chem. Soc.* **127**, 5517 (2005).
[78] M. J. Matthews, M. A. Pimenta, G. Dresselhaus, M. S. Dresselhaus, M. Endo. *Phys. Rev. B Condens. Matter Mater. Phys.* **59**, R6585 (1999).
[79] C. Casiraghi, S. Pisana, K. S. Novoselov, A. K. Geim, A. C. Ferrari. *Appl. Phys. Lett.* **91**, 233108 (2007).
[80] I. Y. Jeon, H. J. Choi, S. M. Jung, J. M. Seo, M. J. Kim, L. Dai, J. B. Baek. *J. Am. Chem. Soc.* **135**, 1386 (2012).